Lawrence Berkeley National Laboratory
Lawrence Berkeley National Laboratory

Title

Imaging of InGaN inhomogeneities using visible apertureless near-field scanning optical microscope

Permalink
https://escholarship.org/uc/item/48f5981t

Authors
Stebounova, Larissa V.
Romanyuk, Yaroslav E.
Chen, Dongxue
et al.

Publication Date
2007-06-14

Peer reviewed

eScholarship.org Powered by the California Digital Library
University of California

Imaging of InGaN inhomogeneities using visible apertureless near-field scanning optical microscope

Larissa V. Stebounova, Yaroslav E. Romanyuk, Dongxue Chen,[a] and Stephen R. Leone[b]

Departments of Chemistry and Physics, University of California, and Lawrence Berkeley National Laboratory, Berkeley, California 94720

Received (

The optical properties of epitaxially grown islands of InGaN are investigated with nanometer-scale spatial resolution using visible apertureless near-field scanning optical microscopy. Scattered light from the tip-sample system is modulated by cantilever oscillations and detected at the third harmonic of the oscillation frequency to distinguish the near-field signal from unwanted scattered background light. Scattered near-field measurements indicate that the as-grown InGaN islanded film may exhibit both inhomogeneous In composition and strain-induced changes that affect the optical signal at 633 nm and 532 nm. Changes are observed in the optical contrast for large 3D InGaN islands (100's of nm) of the same height. Near-field optical mapping of small grains on a finer scale reveals InGaN composition or strain-induced irregularities in features with heights of only 2 nm, which exhibit different near-field signals at 633 nm and 532 nm incident wavelengths. Optical signal contrast from topographic features as small as 30 nm is detected.

---

[a] Present address: Luminescent Technologies, Inc., 2471 East Bayshore Road, Palo Alto, CA 94303

[b] Corresponding author; e-mail: srl@berkeley.edu; Fax 1-510-6431376

Introduction

The direct bandgap of InGaN alloys covers the entire visible spectral region, even providing near-infrared and ultraviolet components, which allows building optical devices operating over this entire wavelength range. InGaN-based light emitting diodes in near UV and visible range and violet laser diodes are already commercially available, taking advantage of the very high light emission efficiency of this material.[1,2] The growth of nitride semiconductors on lattice-mismatched substrates causes the formation of various defects, especially dislocations, which affect the luminescence efficiency because they serve as nonradiative recombination centers.[3] Although devices with excellent performance are achieved, the correlations between the In/Ga composition variations, defects, strain, and optical properties are still not fully understood.

The large difference in the lattice constants of GaN and InN (~11%) gives rise to a solid phase miscibility gap in the GaN-InN alloy system.[4] Therefore, phase segregation and compositional fluctuations in the InGaN alloy system are detected by many researchers.[5-8] Emission from undoped InGaN is sometimes attributed to the recombination of excitons localized at potential minima originating from the phase-segregated In-rich regions.[9] Moreover, direct observation of self-formed quantum dots in InGaN is demonstrated using high resolution transmission electron microscopy[10] and it is found that In composition in dot-like regions is larger then in the neighboring regions using energy dispersive X-ray (EDX) microanalysis.[11] The average size of self-formed InN-rich quantum dots is in the range of 2-5 nanometers.[10, 11] Localized excitons dominate the emission in the case of complete phase separation of InGaN.[12] Emission

from InGaN quantum dots is detected at room temperature and quantum dots can serve as centers for exciton localization and recombination.[13]

Other investigations into the origins of various luminescence properties of InGaN consider strain and structural aspects. Changes in photoluminescence spectra depend on the location where they are collected, and the presence of double luminescence peaks in InGaN is linked to spatially segregated 2D (strained) and 3D (relaxed) growth of InGaN on a microscopic scale, not just to variations in the alloy's composition.[14] Spatially resolved optical studies may provide further insights into how structural and compositional variations influence the optical properties of nitride semiconductors. Due to the small degree of possible compositional variations in InGaN, near-field scanning optical microscopy is a valuable technique to investigate the correlation between spatial inhomogeneities and optical contrast in InGaN.

Scanning near-field optical microscopy is a powerful tool for optical investigation of a material's properties on the nanoscale. High spatial resolution is achieved by detecting evanescent fields present at the sample surface.[15] Apertureless near-field scanning optical microscopy (ANSOM) usually employs a sharp metallic or dielectric probe tip to re-radiate evanescent components of the electromagnetic field excited at the surface of a sample by laser light.[16-18] A lateral spatial resolution of less than 30 nm in visible ANSOM is reported for nitride semiconductor surfaces, which is limited by the size of the probe.[19, 20] There are several investigations of imaging submicron distributions of photo- and electro-luminescence intensities from InGaN/GaN quantum structures by near-field microscopy.[21-27] An inhomogeneous distribution of photoluminescence from InGaN/GaN quantum wells is observed.[22-25] The spatial resolution in these studies is

≥100 nm due to the size of the aperture probe. Time-resolved near-field studies identify radiative and nonradiative centers in samples.[24, 25] While some results of near-field microscopy photoluminescence imaging indicate that there is not a strong localization of carriers in InGaN, the results of near-field studies of electroluminescence[26, 27] point out that the effect of carrier localization influences the luminescence properties of InGaN-based devices. A spatial resolution of a few nanometers is needed to identify such localization centers in both topography and optical images.

In this study, the optical properties of an islanded InGaN film are investigated by apertureless near-field scanning optical microscopy (ANSOM) at two different visible wavelengths, 633 nm and 532 nm. Wavelength-dependent near-field signal changes are observed for both large and small island structures. The results suggest that both compositional and structural variations in the InGaN alloy may be responsible for different optical contrasts in the near-field signal maps on the nanoscale.

Experiments

An islanded InGaN film is grown by molecular beam epitaxy (MBE) in a home-built MBE chamber with a base pressure of 10^{-8} Pa. Indium and gallium are evaporated from Knudson cells and the beam fluxes are calibrated using a quartz crystal microbalance. An active nitrogen flux is generated by a radio-frequency (RF) plasma source. The sample surface crystal structure and chemical composition are examined by low energy electron diffraction (LEED), Auger electron spectroscopy and X-ray diffraction (Siemens D-500 diffractometer). Topography of the as-grown samples is analyzed after growth with an

atomic force microscope (AFM) (Multimode, Digital Instruments), as well as with the ANSOM apparatus, described in detail below.

Sapphire substrates are prepared as described previously.[28] A GaN buffer layer is grown after the nitridation of the substrate. A Ga/N flux ratio at (or slightly above) one is used to achieve smooth GaN surfaces. Details of the GaN growth are also reported previously.[28] InGaN is deposited on the GaN buffer layer at a temperature of 550 °C keeping the nitrogen pressure at 2×10^{-3} Pa and the RF power at 300 W. In and Ga fluxes of 1.3 nm/min and 6.7 nm/min, respectively, are supplied to the MBE chamber. After 90 min of growth, the InGaN film thickness is about 0.5 μm. AFM images of the sample reveal the formation of 3D islands, which display flat top surfaces. The average height of the islands is ~75 nm and the lateral sizes are a few hundred nanometers for the bigger islands, as measured from AFM line scans. An average In content of 14% in the as-grown InGaN film is determined by X-ray diffraction (insert in Fig. 1) assuming that both the InGaN and GaN films are relaxed and Vegard's law can be applied.[29]

Optical properties of the sample are examined by photoluminescence (PL) spectroscopy and near-field microscopy. A He-Cd continuous-wave laser beam at 325 nm with a power of 30 mW is used to perform optical excitation of the sample for the PL measurements. The luminescence spectra are detected by a photomultiplier tube and analyzed by a 0.85 m double-grating spectrometer (Spex 1404).

The ANSOM apparatus built in our laboratory is based on a commercial AFM scanner head (Bioscope, Veeco Instruments). The AFM scanner head is controlled by a separate electronics control system (SPM 1000, RHK Technology) and feedback in intermittent-contact mode is achieved by comparing the amplitude of the cantilever

oscillations to a setpoint using a lock-in amplifier (SR830, Stanford Research Systems). An AFM silicon tip (MicroMasch, typical tip curvature radius < 10 nm) is oscillated at a resonance frequency of about 60 kHz near the sample surface. Linearly polarized radiation from a HeNe laser (633 nm, Micro-g Inc.) or frequency-doubled Nd:YAG cw laser (532 nm, CrystaLaser) is directed into a microscope objective lens (0.42 NA, 20X, Mitutoyo) and focused onto the sample at an angle of 30° with respect to the sample surface. Back scattered radiation from the tip-sample junction is collected by the same objective lens. A schematic drawing of the basic optical components for near-field measurements was presented previously.[19] Homodyne amplification is not used in these experiments, although it provides better discrimination against topographic artifacts.[19] One possible source of the topography contribution in the near-field signal could be due to the surface reflections of the incident light interfering with each other and with the near-field signal. Since the sample is stationary in our setup, we believe that this self-homodyning effect does not create topography artifacts in the near-field signal. The signal detected by the photodiode contains a large far-field scattered background that originates from the sample surface and tip shaft. This background is almost completely removed by demodulating the signal at the third harmonic of the tip oscillation frequency using a wide-band lock-in amplifier (7820 model, Signal Recovery). Optical and topography images of the sample are recorded simultaneously.

Results and Discussion

Photoluminescence measurements from different locations of the InGaN sample demonstrate broad double peak spectra, a wide peak at around 480-520 nm and a shoulder at around 400-420 nm (Fig. 1). These observations are consistent with photoluminescence results reported in the literature for similar samples.[14] The difference in PL spectra collected from different locations of the sample (Fig. 1) indicates that our sample is inhomogeneous. The broadened X-ray diffraction peak seen in the insert in Fig. 1 is another indication of compositional fluctuations within the sample. Compositional variations in our sample are possible because the Ga flux drifted during the sample growth, causing different incorporation rates for Ga and In.

Double peak PL spectrum can be indicative of phase separation in the alloy. Dependences of the absorption edge and luminescence energy on the mole fraction of In in an InGaN alloy have been previously reported.[30, 31] The indium content, which corresponds to the 420 nm PL peak position is ~10-15%, and this agrees very well with the indium fraction obtained from X-ray diffraction (~14%). The stronger peak at 480-520 nm corresponds to the indium content of ~15-20%, which is also possible in our sample.

Another possible origin of the two peaks in the PL spectrum also needs to be considered. Usually images of spatially resolved luminescence display PL variations on several hundred nanometer length scales, which is often correlated with the distributions of radiative/non-radiative centers in the alloy.[22-25] Correlations between structural and luminescence properties of thick InGaN layers can originate in the transition from 2D to 3D growth mode taking place after the critical layer thickness (CLT).[32] The splitting in the PL spectrum collected from InGaN layers grown above the CLT can be related to the

variations in the strain-field-originated 2D/3D growth transition.[14] Double peaks in the PL spectrum may represent the signal from the relaxed, 3D region of the sample (strong peak at ~480-520 nm), and the signal from the strained layer close to the GaN/InGaN interface may be represented as a smaller peak shifted to higher energies in Fig. 1. We have observed such PL behavior in other InGaN samples exihibiting 3D island surface morphology.

Near-field signal maps of InGaN islands were collected under excitation by two different laser wavelengths. Figure 2 shows AFM topography and ANSOM images (third harmonic intensity) collected at 633 nm and 532 nm excitation wavelengths. The InGaN sample consists of many large islands with a lateral size of a few hundred nanometers as can be seen from the topography image. The relative heights of the islands determined from the AFM images are in the range of 60-90 nm. There are a few tall features in the topography image that appear as white spots in Fig 2(a). These are more than 2 times higher than the average island height and most likely represent contamination of the sample surface. A large contrast change for these tall features is observed in the near-field images in Figs. 2(b) and 2(c). Such a large contrast change is due to a large change in dielectric constant of the material,[19, 33, 34] which also confirms that they have a different chemical composition than the rest of the sample.

We observe a signal enhancement in the near-field images in Fig. 2 that is detected as white stripes on the right sides of the islands. We attribute this signal change to the sudden change in the vertical tip position during scanning, since the position of the enhanced signal depends on the direction in which the sample is scanned. The sample is scanned from the left to the right in the displayed images. A similar signal enhancement

occurs on the left sides of the islands when the sample is scanned in the opposite direction (not shown). A possible mechanism for this effect has been discussed[35] and can be described with the aid of Fig. 3. After scanning the flat top of an island the tip reaches the island's edge. The forces acting on the tip by the sample start decreasing, which causes the tip to jump towards the surface and thus the amplitude of the cantilever oscillations will momentarily increase. The increase in the amplitude leads to an increase in the near-field signal near the sample surface, since the optical signal decays exponentially with the distance away from the surface. In other words, the harmonicity of the cantilever motion is locally perturbed and an anharmonic cantilever motion can create an artifact in the optical signal.[35, 36] Fig. 3 displays cross sections of the topography and near-field signal images. A correlation between near-field signal jump at the edge of the island and a possible increase in the cantilever's oscillation amplitude is schematically represented. After going over the edge of an island the AFM feedback adjusts the position of the cantilever to maintain constant amplitude during scanning.

It can be noted from the near-field images in Fig. 2 that the near-field signal level varies from island to island for islands of the same height and also for the same islands in the images collected at the two different incident wavelengths, 633 nm and 532 nm. These results apply to the islands within the normal height range (not the brightest white zones in the topography). To see this better, line scans along the dashed lines in the images in Fig. 2 are plotted in Fig. 4. Similar effects are observed all over the sample. Height profiles are represented by the light grey lines and it can be seen that the islands are approximately of the same height of 70-80 nm. The dark grey lines represent near-field signal line scans. The line scans in Figs. 4(a) and 4(b) were collected at the same

positions on the sample with 633 nm and 532 nm, respectively. Interestingly, the near-field signal is smaller for the last two islands, marked by the arrows, in the line scan at 633 nm, while it remains at a similar level for all islands in the line scan obtained for 532 nm. It was noted above that the structure and optical properties of thick InGaN films can change due to strain variations in the sample. 2D growth of InGaN initiated on a GaN buffer layer produces a strained material with multiple defects in the crystal lattice, while 3D growth originating from strained layers produces a relaxed material with characteristic 3D islands, *via* the Stranski-Krastanow mechanism. AFM and ANSOM topography images of our sample clearly display 3D structure, which means that the 2D/3D transition has occurred. The critical layer thickness at which strain relief is predicted to occur for an $In_{0.14}Ga_{0.86}N$ film is 60 nm.[32] We estimate the thickness of the 3D layer to be in the range of 400-600 nm. Although near-field probing is not sensitive at a depth of 500 nm, which would reach the 2D layer, the structural and compositional properties of the sample can vary just below the sample's surface. It has been observed that variations in vertical composition of a sample can influence near field optical signals.[37, 38] Since both compositional fluctuations and structural variations are possible in our sample, the near-field signal variations in the near-field signal maps in Figs. 2(b) and 2(c) can be due to either or both of these two effects. The larger crystalline islands in Fig. 2 are more likely to exhibit near-field signal changes due to strain-induced effects since we do not have direct evidence for macroscopic phase separation of the InGaN alloy in the sample, such as an additional X-ray diffraction peak, although we cannot rule out compositional variations induced by strain variations.

We now examine the morphology of the InGaN islands at a smaller spatial scale. We find that the large flat islands in Fig. 2(a) actually have small grains of a few nanometers in height on their surface. An example of such topography is shown in Fig. 5(a), which corresponds to the area marked by the white square in Fig. 2(a). The grains are approximately 2 nm in height. Figs. 5(b) and 5(c) represent near-field signal maps collected from the same area at 633 nm and 532 nm, correspondingly. We observe that the near-field signals from some of the grains change contrast relative to the signal from the neighboring areas depending on the incident wavelength. For example, larger grains marked by the white circles in Fig. 5 display an optical signal decrease in the red (Fig. 5(b)) and a signal increase in the green (Fig. 5(c)) relative to the signal from the surroundings. One of the possible explanations may be that these grains are InN-rich nanoislands. It has been shown that it is energetically favorable for indium to stay on the surface during InGaN film growth by MBE.[39] Surface confinement of an InN-rich phase in thick InGaN films has also been observed by photoluminescence depth profiling.[40] It was found that a PL peak around 2.6 eV disappears after removing the surface layer of ~50 nm from a $In_{15}Ga_{85}N$ sample.[40] This suggests that there may be segregation of the InN-rich regions on the InGaN surface. There is direct evidence that In composition in self-formed nanodots at an InGaN interface measured by energy-dispersive X-ray microanalysis is larger than the In composition of the surrounding alloy.[11] The strain distribution can play a role in the self-formation of quantum dots. For example, misfit dislocations, formed as a result of strain, can induce the self-formation of semiconductor nanodots at the top surface of the semiconductor layer.[41] In addition, small pits formed due to the strain in the surface layer of In can lead to an increasing concentration of In

inside and around the pits.[42] While both strain and In surface segregation can be explanations for the observed surface irregularities in our sample, it is likely that the finer features in Fig. 5 contain higher concentrations of In.

The near-field signal change for red and green illumination wavelengths (Figs. 5(b) and 5(c)) is indicative of the changes in the material's optical properties. The change in the near-field contrast on the grains for different incident wavelengths in Fig. 5 cannot be solely anticipated by the difference in the dielectric constants between surrounding $In_{14}Ga_{86}N$ and possibly InN-rich alloys in the grains. The dielectric constants, for example, of $In_{14}Ga_{86}N$ and $In_{20}Ga_{80}N$ (we consider an indium fraction of 0.2 in the InN-rich regions as an example, but we do not know the exact composition of the grains) do not change significantly at 633 nm and 532 nm (Table I).[43] A near-field size-dependent contrast reversal was observed at 633 nm excitation wavelength for InGaN dots deposited on a GaN substrate.[44] In that work, it is predicted that tip-substrate dipolar coupling overrides tip-particle dipolar coupling for particles smaller than the size of the tip. The lateral sizes of the grains observed in Fig. 5 (~30-50 nm) are comparable to the realistic size of the tip (the tip becomes dull very quickly and usually has a larger radius of curvature than specified by manufacture); the actual lateral sizes of our grains might be significantly smaller due to the convolution of the tip shape with the grain shape,[45] therefore it is uncertain whether dipolar coupling between the tip and the neighboring InGaN regions influences the near-field signal from the grains. Since the dielectric constants of the grains and neighboring regions vary insignificantly at the same wavelength (Table I), we assume that the near-field signal change on the grains is not affected by the tip-substrate dipolar coupling. The influence of the vertical structural and

compositional fluctuations of the sample on the near-field signal contrast at different wavelengths needs to be considered in future near-field signal modeling.

Other processes might be responsible for the near-field signal increase from InN-rich regions at 532 nm. For example, a larger optical signal at 532 nm could be caused by an enhanced recombination of excitons in the InN-rich regions because of the higher excitation efficiency of InGaN at 532 nm compared to the excitation efficiency at 633 nm. Spectrally-resolved near-field measurements need to be done to conclude whether exciton localization occurs in the inhomogeneities observed in Fig. 5. Different designs of scanning near-field optical microscopes have been used to observe tip-enhanced fluorescence of quantum dots,[46] to collect PL spectra of single semiconductor nanocrystals,[47] to obtain Raman spectra of an individual single wall carbon nanotubes,[48] and to acquire spatially-resolved electro-luminescence spectra of InGaN multiple quantum wells.[27] Low-temperature near-field luminescence spectroscopy could give an insight into whether self-organized In-rich regions serve as the radiation recombination centers.[27] Other methods, such as EDX can be used to determine the exact composition of the grains and whether it is different from the surrounding areas. We believe both strain variations in the sample and fluctuations of indium in the alloy composition could be responsible for the observed near-field contrast on the small dots.

Conclusions

We use apertureless near-field scanning optical microscopy to study optical and structural properties of InGaN films with nanoscale spatial resolution superior to the resolution

obtained by other groups that investigated photoluminescence properties of InGaN using aperture probe near-field microscopy. We observe variations in the optical signal from grains as small as 30 nm in diameter. Near-field imaging of the InGaN film reveal that some islands formed during the 3D growth mode display different near-field signal than the others. Compositional and structural variations in InGaN films contribute to the near-field signal contrast. We observe small surface irregularities on the "flat" surfaces of large InGaN islands that show clear near-field contrast differences at 633 nm and 532 nm incident wavelengths. It may indicate that the In composition of these surface grains is different from the In composition of the surrounding areas. Other methods, such as energy-dispersive X-ray analysis are needed to determine the composition of the grains observed on the InGaN surface.

AKNOWLEDGMENTS

This work was supported by the Director, Office of Science, Office of Basic Energy Sciences, of the U.S. Department of Energy under Contract No. DE-AC02-05CH11231 and by the National Science Foundation under Grant No. NSF-DMR-0302446.

References

1. S. Nakamura, M. Senoh, N. Iwasa, and S. Nagahama, Jpn. J. Appl. Phys. **34** L797 (1995).
2. S. Nakamura, M. Senoh, S. Nagahama, T. Matsushita, H. Kiyoku, Y. Sugimoto, T. Kozaki, H. Umemoto, M. Sanoh, and T. Mukai, Jpn. J. Appl. Phys. **38** L226 (1999).
3. N. Yamamoto, H. Itoh, V. Grill, S. F. Chichibu, S. Keller, J. S. Speck, S. P. DenBaars, U. K. Mishra, S. Nakamura, and G. Salviati, J. Appl. Phys. **94**, 4315 (2003).
4. I-hsiu Ho and G. B. Stringfellow, Appl. Phys. Lett. **69**, 2701 (1996).
5. A. Wakahara, T. Tokuda, X. Dang, S. Noda, and A. Sasaki, Appl. Phys. Lett. **71**, 906 (1997).
6. Z. Liliental-Weber, D. N. Zakharov, K. M. Yu, J. W. Ager III, W. Walukiewicz, E. E. Haller, H. Lu, and W. J. Schaff, Physika B **376-377**, 468 (2006).
7. R. Singh, D. Doppalapudi, T. D. Moustakas, and L. T. Romano, Appl. Phys. Lett. **70**, 1089 (1997).
8. N. A. Al-Masry, E. L. Piner, S. X. Liu, and S. M. Bedair, Appl. Phys. Lett. **72**, 40 (1998).
9. S. Chichibu, T. Azuhata, T. Sota, and S. Nakamura, Appl. Phys. Lett. **70**, 2822 (1997).
10. L. Nistor, H. Bender, A. Vantomme, M. F. Wu, J. Van Landuyt, K. P. O'Donnell, R. Martin, K. Jacobs, and I. Moerman, Appl. Phys. Lett. **77**, 507 (2000).

11. Y. Narukawa, Y. Kawakami, M. Funato, S. Fujita, S. Fujita, and S. Nakamura, Appl. Phys. Lett. **70**, 981 (1997).

12. P. Chen, S. J. Chua, and Z. L. Miao, J. Appl. Phys. **93**, 2507 (2003).

13. C. Adelmann, J. Simon, G. Feuillet, N. T. Pelekanos, B. Daudin, and G. Fishman, Appl. Phys. Lett. **76**, 1570 (2000).

14. K. P. O'Donnell, S. Pereira, R. W. Martin, P. R. Edwards, M. J. Tobin, and J. F. W. Mosselmans, Phys. Status Solidi A **195**, 532 (2003).

15. D. Courjon and C. Bainier, Rep. Prog. Phys. **57**, 989 (1994).

16. J. Wessel, J. Opt. Soc. Am. B **2**, 1538 (1985).

17. F. Zenhausern, Y. Martin, and H. K. Wickramasinghe, Science **269**, 1083 (1995).

18. B. Knoll and F. Keilmann, Nature **399**, 134 (1999).

19. Z. H. Kim, B. Liu, and S. R. Leone, J. Phys. Chem. B **109**, 8503 (2005).

20. Z. H. Kim and S. R. Leone, J. Phys. Chem. B **110**, 19804 (2006).

21. M. Labardi, P. G. Gucciardi, M. Allegrini, and C. Pelosi, Appl. Phys. A **66**, S397 (1998).

22. P. A. Crowell, D. K. Young, S. Keller, E. L. Hu, and D. D. Awschalom, Appl. Phys. Lett. **72**, 927 (1998).

23. M. S. Jeong, J. Y. Kim, Y.-W. Kim, J. O. White, E.-K. Suh, C.-H. Hong, and H. J. Lee, Appl. Phys. Lett. **79**, 976 (2001).

24. A. Kaneta, K. Okamoto, Y. Kawakami, S. Fujita, G. Marutsuki, Y. Narukawa, and T. Mukai, Appl. Phys. Lett. **81**, 4353 (2002).

25. A. Kaneta, T. Mutoh, S. Fujita, G. Marutsuki, Y. Narukawa, and T. Mukai, Appl. Phys. Lett. **83**, 3462 (2003).

26. G. Marutsuki, Y. Narukawa, T. Mitani, T. Mukai, G. Shinomiya, A. Kaneta, Y. Kawakami, and S. Fujita, Phys. Status Solidi A **192**, 110 (2002).

27. G. Xu, W. Zhang, X. Zhu, H. Liang, Y.-D. Qi, and K. M. Lau, J. Kor. Phys. Soc. **47**, S109 (2005).

28. B. Liu, T. Kitajima, D. Chen, and S. R. Leone, J. Vac. Sci. Technol. A **23**, 304 (2005).

29. K. P. O'Donnell, J. F. W. Mosselmans, R. W. Martin, S. Pereira, and M. E. White, J. Phys.: Condens. Matter **13**, 6977 (2001).

30. S. Srinivasan, F. Bertram, A. Bell, F. A. Ponce, S. Tanaka, H. Omiya, and Y. Nakagawa, Appl. Phys. Lett. **80**, 550 (2002).

31. K. P. O'Donnell, R. W. Martin, C. Trager-Cowan, M. E. White, K. Esona, C. Deatcher, P. G. Middleton, K. Jacobs, W. Van der Stricht, C. Merlet, B. Gil, A. Vantomme, and J. F. W. Mosselmans, Mat. Sci. Eng. B **82**, 194 (2001).

32. S. Pereira, Thin Solid Films **515**, 164 (2006).

33. B. Knoll and F. Keilmann, Nature **399**, 134 (1999).

34. B. B.Akhremitchev, Y. Sun, L. Stebounova, and G. C. Walker, Langmuir **18**, 5325 (2002).

35. L. Billot, M. Lamy de la Chapelle, D. Barchiesi, S.-H. Chang, S. K. Gray, J. A. Rogers, A. Bouhelier, P.-M. Adam, J.-L. Bijeon, G. P. Wiederrecht, R. Bachelot, and P. Royer, Appl. Phys. Lett. **89**, 023105 (2006).

36. A. Bek, R. Vogelgesang, and K. Kern, Appl. Phys. Lett. **87**, 163115 (2005).

37. M. B. Raschke and C. Lienau, Appl. Phys. Lett. **83**, 5089 (2003).

38. T. Taubner, F. Keilmann, and R. Hillenbrand, Opt. Express **13**, 8893 (2005).

39. H. Chen, R. M. Feenstra, J. Northrup, J. Neugebauer, and D. W. Greve, MRS Internet J. Nitride Semicond. Res. **6**, 11 (2001).

40. T.-S. Kim, S.-W. Kim, H.-K. Kim, and J.-M. Lee, Superlattices Microstruct. **40**, 545 (2006).

41. T. Kanto and K. Yamaguchi, Jpn. J. Appl. Phys. **44**, 7690 (2005).

42. H. Chen, R. M. Feenstra, J. E. Northrup, T. Zywietz, J. Neugebauer, and D. W. Greve, J. Vac. Sci. Technol. B **18**, 2284 (2000).

43. R. Goldhahn, Acta Phys. Pol. A **104**, 123 (2003).

44. Z. H. Kim, S.-H. Ahn, B. Liu, and S. R. Leone, submitted to Nano Letters (2007).

45. H.-J. Butt, R. Guckenberger, and J. P. Rabe, Ultramicroscopy **46**, 735 (1992).

46. J. M. Gerton, L. A. Wade, G. A. Lessard, Z. Ma, and S. R. Quake, Phys. Rev. Lett. **93**, 180801 (2004).

47. A. Ishizumi, K. Matsuda, T. Saiki, C. W. White, and Y. Kanemitsu, Appl. Phys. Lett. **87**, 133104 (2005).

48. N. Anderson, A. Bouhelier, and L. Novotny, J. Opt. A: Pure Appl. Opt. **8**, S227 (2006).

Table I. Wavelength-dependent complex dielectric constants of InGaN[43]

Alloy	633 nm	532 nm
$In_{14}Ga_{86}N$	5.76+0.33i	5.77+0.33i
$In_{20}Ga_{80}N$	5.83+0.48i	5.82+0.48i

List of Figure Captions:

FIG. 1. Photoluminescence spectra of InGaN film collected at two different locations of the sample. The insert shows X-ray diffraction reflection from the (006) crystallographic plane for the InGaN layer and GaN buffer (both Cu$K\alpha_1$ and Cu$K\alpha_2$ lines are visible for the GaN reflection).

FIG. 2. (a) Topography of InGaN sample obtained by the ANSOM apparatus. The average height of the islands is about 60-90 nm. (b) and (c) Near-field signal maps collected at the third harmonic of the cantilever's oscillation frequency under 633 nm and 532 nm excitation, respectively.

FIG. 3. Cross sections of the topography (light grey line) and near-field signal (dark grey line) images from Figs. 2(a) and 2(b), respectively. The schematic positions of the AFM tip relative to the sample surface and AFM setpoint indicate an increase in cantilever oscillation amplitude at an edge of the island where an increase of the near-field signal is also observed.

FIG. 4. (a) Cross sections of the topography (light grey) and near-field signal (dark grey) collected at 633nm. (b) Cross sections of the topography (light grey) and near-field signal (dark grey) collected at 532nm. Near-field signal contrast changes at 633 nm for the islands marked by the arrows.

FIG. 5. Topography (a) and near-field images collected at 633 nm (b) and 532 nm (c) of single InGaN island in the square marked on Fig. 2. Topography grains with a height of ~2 nm indicated by white circles display opposite contrast in near-field images collected at different wavelengths. Grey scale bar next to the topography image indicates a relative grey scale for the heights. Image size is approximately 380 nm.

Figure 1 Stebounova *et al.* J. Appl. Phys.

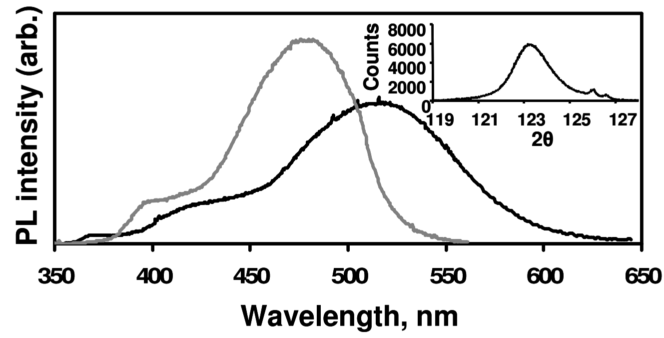

Figure 2 Stebounova *et al.* J. Appl. Phys.

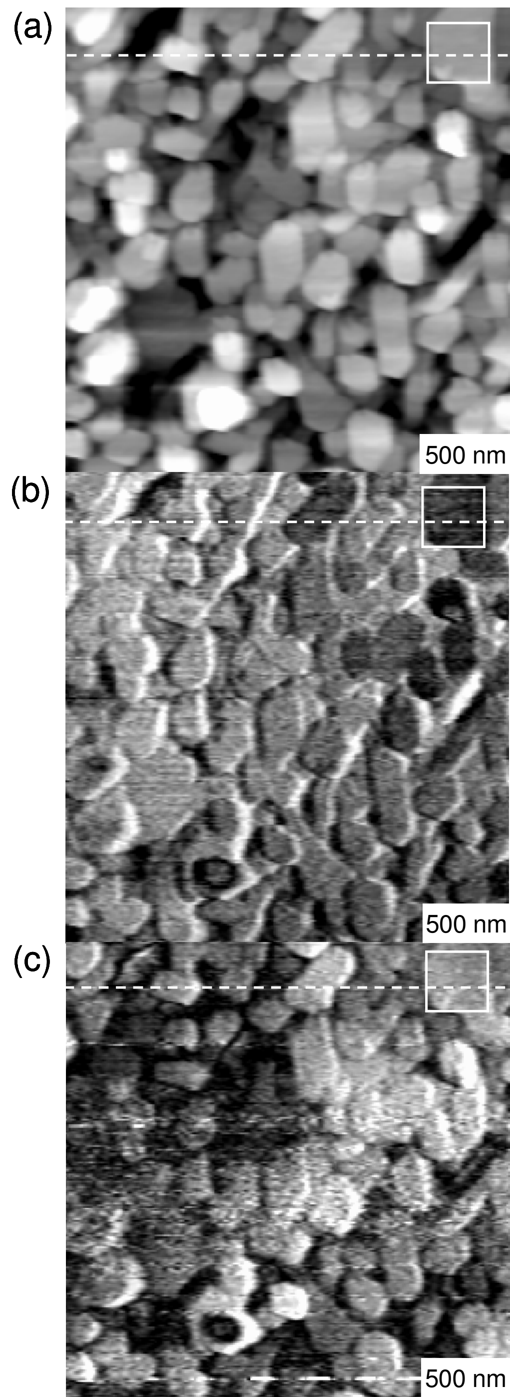

Figure 3 Stebounova *et al.* J. Appl. Phys.

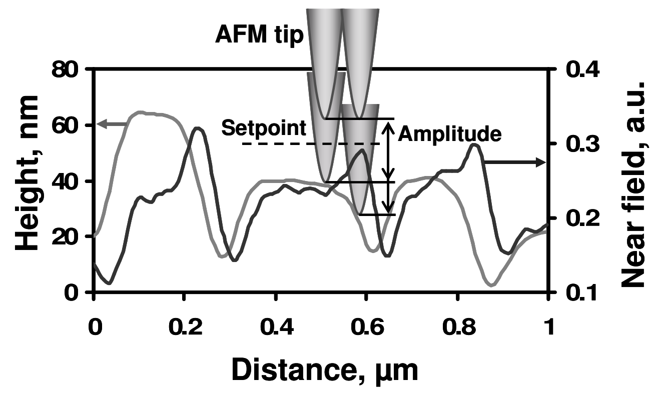

Figure 4 Stebounova *et al.* J. Appl. Phys.

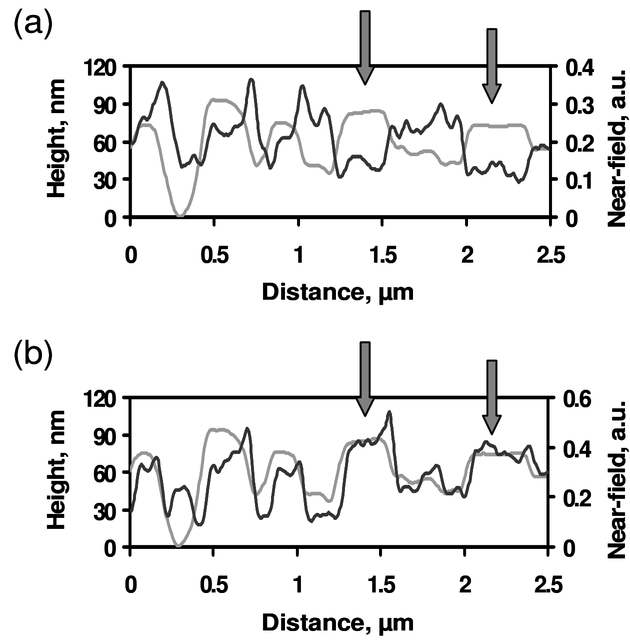

Figure 5 Stebounova *et al.* J. Appl. Phys.